BRIEF COMMUNICATION

Blood plasma derived extracellular vesicles (BEVs): particle purification liquid chromatography (PPLC) and proteomic analysis reveals BEVs as a potential minimally invasive tool for predicting response to breast cancer treatment

Folnetti A. Alvarez[1] · Hussein Kaddour[1,2] · Yuan Lyu[1,3] · Christina Preece[4,5] · Jules Cohen[6,7] · Lea Baer[6,7] · Alison T. Stopeck[6,7] · Patricia Thompson[4,7] · Chioma M. Okeoma[1,8]

Abstract

Purpose Circulating blood plasma derived extracellular vesicles (BEVs) containing proteins hold promise for their use as minimally invasive biomarkers for predicting response to cancer therapy. The main goal of this study was to establish the efficiency and utility of the particle purification liquid chromatography (PPLC) BEV isolation method and evaluate the role of BEVs in predicting breast cancer (BC) patient response to neoadjuvant chemotherapy (NAC).

Methods PPLC isolation was used to separate BEVs from non-EV contaminants and characterize BEVs from 17 BC patients scheduled to receive NAC. Using LC–MS/MS, we compared the proteome of PPLC-isolated BEVs from patients ($n = 7$) that achieved a pathological complete response (pCR) after NAC (responders [R]) to patients ($n = 10$) who did not achieve pCR (non-responders [NR]). Luminal MCF7 and basaloid MDA-MB-231 BC cells were treated with isolated BEVs and evaluated for metabolic activity by MTT assay.

Results NR had elevated BEV concentrations and negative zeta potential (ζ-potential) prior to receipt of NAC. Eight proteins were enriched in BEVs of NR. GP1BA (CD42b), PECAM-1 (CD31), CAPN1, HSPB1 (HSP27), and ANXA5 were validated using western blot. MTT assay revealed BEVs from R and NR patients increased metabolic activity of MCF7 and MDA-MB-231 BC cells and the magnitude was highest in MCF7s treated with NR BEVs.

Conclusion PPLC-based EV isolation provides a preanalytical separation process for BEVs devoid of most contaminants. Our findings suggest that PPLC-isolated BEVs and the five associated proteins may be established as predictors of chemoresistance, and thus serve to identify NR to spare them the toxic effects of NAC.

Keywords BEVs · PPLC · Breast cancer · Neoadjuvant chemotherapy · Chemoresistance · Biomarkers

Introduction

Extracellular vesicles (EVs) are heterogeneous populations of cell derived membrane vesicles with different sizes and origins. Microvesicles, exosomes, and apoptotic bodies are subsets of EVs which can be distinguished by their size, density, structure, and cargo composition (surface markers, and luminal cargo), however, some of these features are overlapping. EVs carry several molecules (cargoes), including DNA, RNA, protein, drugs, and pathogen products [1–19]

that act to protect these molecules from the extracellular milieu. It has been shown that cancer cells [20, 21] and the blood of cancer patients [22–24] typically produce more EVs compared to normal cells and healthy patients, respectively. Interest in cancer EV-associated biomolecules stem from their complex role in neoplasia, tumor progression, metastasis, and for their potential use as tumor biomarkers [25–27]. Altered enrichment of RNA and protein in EVs reported in cancer and other diseases [28–36] suggest that EVs may serve as disease biomarkers. Several features of blood plasma derived EVs (BEVs) including their abundance (up to 10^{10} EVs/mL of blood), stability, cargo content, potential to inform on real-time state of the producer cells/hosts, and their accessibility for longitudinal sampling make

✉ Chioma M. Okeoma
    chioma.okeoma@stonybrook.edu; cokeoma@nymc.edu

Extended author information available on the last page of the article

them particularly attractive as disease biomarkers for use in the diagnostic setting and in monitoring patient response and resistance to therapy.

Given the potential biological and clinical importance of EVs, preanalytical processing of samples including high quality and reproducible EV isolation methods that eliminates impurities has proven an important criterion for their study. Current EV isolation methods such as differential ultracentrifugation, precipitation, ultrafiltration, density gradient, flow cytometry, immunocapture, microfluidic isolation, and asymmetric flow field flow fractionation (AF4) [37–41] suffer difficulties in recovery of EVs as single, functional vesicles and preparative quantities that support downstream investigation and use without interference of extracellular contaminants. These EV isolation methods exhibit low specificity because they are unable to separate EVs from contaminants, such as lipoproteins and biomolecular membraneless condensates (MCs) [1, 42, 43]. Indeed, lipoproteins, including high-density lipoproteins (HDL) and low-density lipoproteins (LDL) have similar size and density range as EVs. For example, exosomes, a type of EVs range in size from 30 to 150 nm [8], which fall within the size ranges of HDLs (as small as 10 nm), LDLs (20 nm to 200 nm), and smaller chylomicrons (70–1000 nm). In addition, the density of exosomes is between 1.15 g/mL and 1.2 g/mL, which falls within the range of HDL densities of 1.06–1.21 g/mL [44]. Thus, need for preanalytical methods to separate EVs from other molecules prior to their study and characterization and ultimately any use in diagnostics is now well recognized. Moreover, establishing rigorous preanalytical conditions will also minimize artifacts introduced by the interference of soluble proteins and improve interlaboratory reproducibility.

Here, we present the results of a novel size-guided Particle Purification Liquid Chromatography (PPLC) [1] method to enable the separation of blood plasma into EVs, lipoproteins, albumin, and MCs. BEVs were isolated from other non-EV blood components to examine the effects of PPLC BEV isolation method prior to proteomic and functional analysis. To further establish the efficiency and utility of the PPLC BEV isolation method for clinical specimens, we isolated BEVs from blood plasma of a discovery cohort of 17 breast cancer patients prior to the receipt of neoadjuvant chemotherapy (NAC) and analyzed their physicochemical properties, proteome, and function. Physicochemical characterization of the patient-derived BEVs showed that patients who responded to chemotherapy or the responder (R) group had significantly reduced BEV concentration and negative zeta potential (ζ-potential) compared to non-responders (NR). LC–MS/MS analysis and validation identified 5 differentially present proteins (DPPs) in NR BEVs compared to R BEVs. Furthermore, using an in vitro model, we show that BEVs isolated from NRs retained functional activity

and increased breast cancer cell metabolic activity. Based on our results, we recommend an efficient BEV isolation method for downstream physicochemical characterization, proteomic and functional studies that may help to expedite standardization of the EV biomarker field.

Methods

Nomenclature

Blood plasma derived extracellular vesicles (BEVs) encompasses all EVs found in the blood plasma of patients, whether they were released from blood cells or any other cells in the body that release EVs into the blood stream.

Plasma isolation from breast cancer patients

Using an Institutional Review Board (IRB) approved sample collection protocol at Stony Brook Medicine, breast cancer patients ($n = 17$) were consented for serial venous blood collections before initiation of NAC. The clinical characteristics of the patients with available sample for this sub-study are shown in Table 1. Whole blood was immediately processed as shown (Fig. 1a). BEVs were isolated from 300 uL of clarified plasma using PPLC (Fig. 1b). The IRB-approved registry is compliant with all relevant ethical regulations regarding research involving human participants. Informed consent was obtained from all individual participants included in the study. Plasma samples were stored at − 80 °C.

Separation of blood plasma components with PPLC

The PPLC gSEC column [1] (Fig. 1) was packed with size-exclusion dextran-based Sephadex™ G-50 fine (17–0042-01), G-75 (17–0050-01), G-100 (17–0060-01) and 2% agarose-based gel filtration Sepharose CL-2B beads from Cytiva (formerly GE healthcare, Marlborough, MA, USA). The column was prepared by layering the beads from the smallest (G-50) to largest (Sepharose CL-2B) in a 25 cm × 0.5 cm Econo-Column® (Bio-Rad, Hercules, CA, USA) at room temperature by gravity. Analytes were eluted with 1 × phosphate-buffered saline (PBS). Fractions were collected in Greiner UV-Star® 96-well plates using a FC204 fraction collector (Gilson, Middleton, WI, USA), with 12 drops per well. UV–Visible spectroscopy (absorbance) and fluorescence of the fractions were measured using a Synergy H1 plate reader. Fractions in each peak shown in the absorbance profiles (Figs. 2, 3) were pooled and stored at − 80 °C. The BEV samples (peak 1) from each donor were thawed once to measure BEV ζ-potential, protein concentrations, EV marker western blots and transmission electron microscopy (TEM) images. They were thawed a second time

Table 1 Patient demographic and clinicopathological features

Characteristic	TOTAL (N = 17)	R (N = 7)	NR (N = 10)
Race			
Caucasian	13	4	9
African American	2	2	0
Hispanic	1	0	1
Asian	1	1	0
Age, years			
< 40	1	0	1
40–49	8	4	4
≥ 50	8	3	5
Menopausal status			
Postmenopausal	7	4	3
Perimenopausal	1	0	1
Premenopausal	9	3	6
Receptor Status			
HR +, HER2 −	5	0	5
HR +, HER2 +	4	3	1
HR −, HER2 +	3	3	0
TN (HR −, HER2 −)	5	1	4
Clinical stage			
II	10	4	6
III	7	3	4
Clinical T stage			
1	3	1	2
2	10	4	6
3	3	1	2
Unavailable	1	1	0
Clinical N stage			
0	10	3	7
1	5	3	2
2	1	0	1
Unavailable	1	1	0
Pathologic stage (AJCC 7th)			
N/A	7	7	0
I	5	0	5
II	4	0	4
Unavailable	1	0	1
Histologic grade (hg)			
1	1	0	1
2	8	3	5
3	8	4	4
Ki-67 score			
≤ 20%	2	0	2
> 20%	13	6	7
Unavailable	2	1	1

for proteomic analysis. They were thawed a third time for proteomic validations by western blot. The samples were re-stored at − 80 °C after each thaw.

Assessment of BEV concentration, size distribution, and surface charge

The concentration and size of BEVs were determined using the PPLC algorithm described previously [1]. In brief, the Wang et al. model [45] was applied which calculates the scattering cross-section of concentric vesicles with an arbituary size, lipid concentration, membrane thickness, or number of layers. The model uses the open-source light-scattering package HoloPy (holopy.readthedocs.io/) and is available on GitHub (https://github.com/anna-wang/vesicle-turbidity). The EV turbidity spectra corresponding to P1 wells (Fig. 2) was calculated from the absorbance measured in the visible range (400–600 nm) with a 5 nm step using the formula previously described [1]. For analysis of the surface charge, BEVs were diluted in 0.1X PBS (1/1000) and ζ-potential measurements were acquired using nanoparticle tracking analysis (NTA) (ZetaView PMX110, v8.04.02, Particle Metrix, Mebane, NC, USA) as previously described [3]. The shutter was kept at 70, and sensitivity was adjusted to 2–4 points below the noise level to capture small particles.

Immunogold labeling and TEM

Equal volumes of BEVs from each group were pooled. 10 µL were spotted onto TEM grids. The grids were placed into blocking buffer for 1 h and then incubated with anti-CD9 (1:500 dilution) at 4 °C overnight. Subsequently, PBS was used to rinse the grids, which were floated on drops of the secondary antibody attached to 10-nm gold particles (AURION) at room temperature for 1.5 h. The grids were rinsed with PBS and placed into 2.5% glutaraldehyde in 0.1 M phosphate buffer for 15 min. Finally, the grids were stained with uranyl acetate and viewed under a Tecnai G2 20 Twin transmission electron microscope (FEI; 200 kV).

LC–MS/MS and data analysis

BEVs from 17 cancer patients were concentrated using amicon ultra-0.5 centrifugal filter units (Millipore Sigma) by centrifuging at 14,000 g for 25 min to remove excess 1 × PBS. The pellets were at 20 ug of BEVs in 100 µl for LC–MS/MS. Protein concentration was determined using the Bradford assay. Before LC–MS/MS, BEV protein samples were denatured in 5% SDS, 100 mM TEAB, sonicated and reduced with 10 mM TCEP for 20 min at 50 °C. Samples were cooled down for 5 min and treated with 25 mM of iodoacetamide for 20 min, at room temperature (RT) in the dark. Samples bound to S-Trap solid phase cartridges as described [46]. Protein precipitates are washed with 90% methanol, 50 mM TEAB and digested with trypsin at 47 °C for two hours and eluted with sequential 50 mM TEAB, 0.2% formic acid and 50% acetonitrile, 0.2% formic acid
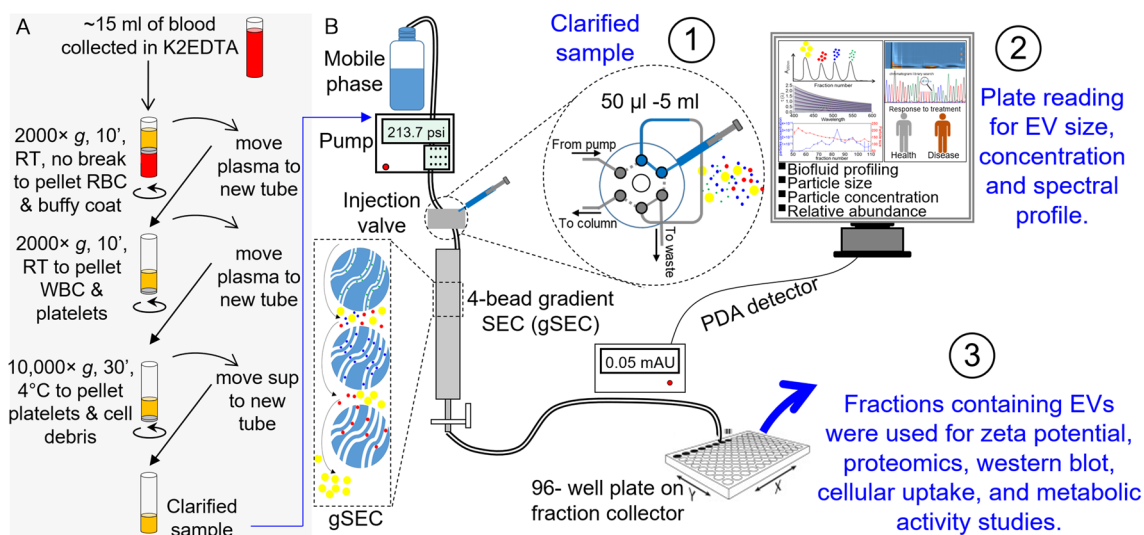
Fig. 1 PPLC for separation of BEVs from other blood plasma particles. **A** Blood plasma clarification. **B** Components of PPLC.

Fig. 2 PPLC efficiently separates BEVs from other blood particles. **A** 280 nm absorbance profile of collected peaks (P1-P3). **B** Collected fractions from P1-P3 probed for EV marker CD9, lipoprotein ApoA1 and albumin (ALB) via western blot and accompanied with silver stain. Numbered lanes represent chosen fraction from corresponding well number from 96-well plates where fractions were collected. **C** 3D spectral profile of P1-P3. **D** Unique spectral signature for each peak distinguishing EVs from other blood particles. **E** TEM images of particles in P1-P3.
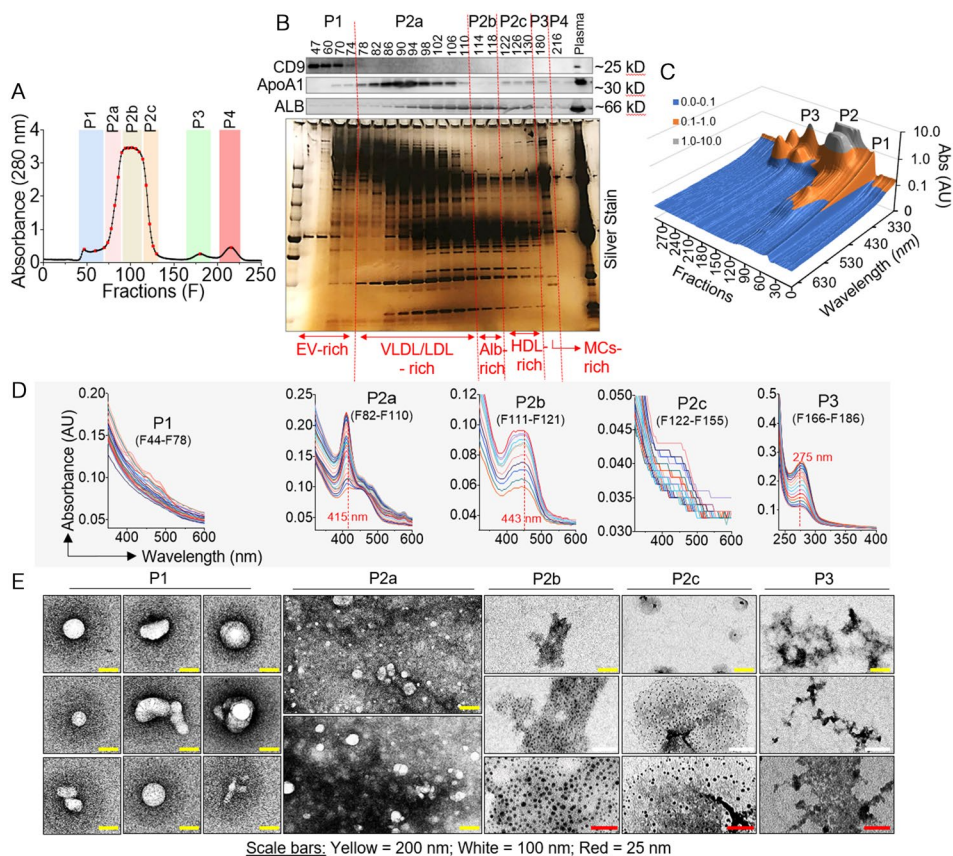
by centrifugation at $4000 \times g$ for 1 min each. Peptides were separated by C18 reverse phase LC–MS/MS. HPLC C18 columns (100 µm ID × 20 cm) were self-packed with 3u Reprosil resin. Peptides were separated using a flow rate of 300 nl/minute, and a gradient elution step changing from 0.1% formic acid to 40% acetonitrile (ACN) over 90 min, followed with 90% ACN wash and re-equilibration steps. Parent peptide mass and collision-induced fragment mass information were collected using an orbital trap (Q-Exactive HF; Thermo) instrument followed by protein database search
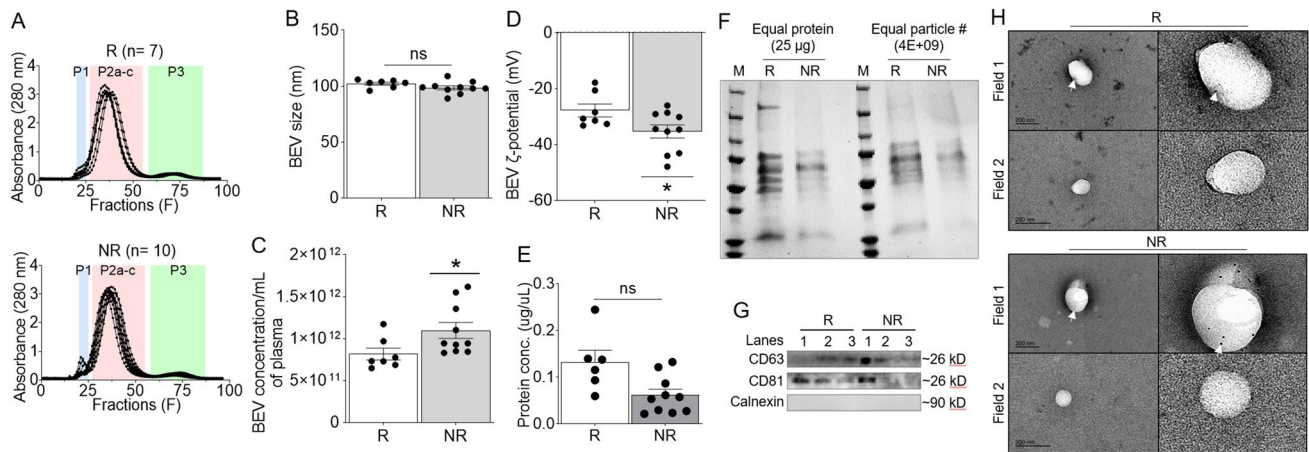
Fig. 3 Biophysical properties of BEVs from breast cancer patients prior to NAC. **A** 280 nm absorbance profile of PPLC peaks (P1-P3) from blood plasma of breast cancer patients with R ($n = 7$) and NR ($n = 10$). **B** BEV size and **C** concentration determined by turbidity spectra measurements. **D** ζ-potential of BEVs measured by Nano Tracking Analysis (NTA). Error bars are SEM of pentaplicate measurements. **E** Protein concentration of BEVs measured by Bradford assay. **F** Western blot protein footprint of pooled (all R patients combined, and all NR patients combined) samples loaded by equal protein and equal particle number **G** Representative western blot of BEV markers CD63 and CD81. Calnexin used as negative control. Lanes R1, 2, 3 each are a pool of 2 different patients (R = 6). Lanes NR 1, 2, 3 each are a pool of 3 different patients (NR = 9). Protein analysis of CD63 and CD81 from individual patients is shown in Supplementary Fig. 1. **H** TEM images of pooled BEVs from 2 different fields of view. Each right-sided image is the left image zoomed in to the BEV that it is directly next to. Arrows indicate CD9-immunogold labeled BEVs. For R and NR, the top left image is at 20kX and the bottom left image is at 30kX. Scale bar: 200 nm. *Unpaired t-test with Welch's correction used to determine differences between groups.* *, $p < 0.05$

using Proteome Discoverer 2.4 (Thermo). Electrospray ionization was achieved using spray voltage of ~ 2.2 kV. Information-dependent MS and MS–MS acquisitions were made using a 100 ms survey scan (m/z 375–1400) at 60,000 resolution, followed typically by 'top 20' consecutive second product ion scans at 15,000 resolution. Peptide and spectra false discovery rates were set to 0.05. Label free quantitation comparisons were performed using spectral counts and precursor abundances.

Western blotting

Equal BEV protein weight (Bradford assay) or particle number (NTA) from both groups were loaded into 4–20% (gradient) Mini-PROTEAN TGX precast gels and resolved by SDS-PAGE at a constant 100 V. The separated proteins were blotted onto PVDF membranes and membranes were blocked with 5% milk dissolved in 1 × TBST (50 mM Tris, 150 mM NaCl, and 0.1% Tween, pH 7.6) buffer for 1 h at room temperature on slow shaker. The membranes were incubated at 4 °C overnight with primary antibodies against CD9 [602.29 cl.11, Developmental Studies Hybridoma Bank (DSHB)], CD63 (H5C6, DSHB), ApoA1 (sc-376818, Santa Cruz), and from proteintech® we used ALB (16,475–1-AP), CD81 (66,866–1-Ig), Calnexin (66,903–1-Ig), CD42b (12,860–1-AP), CD31 (66,065–2-Ig), Calpain 1 (10,538–1-AP), HSP27 (18,284–1-AP), and Annexin V (11,060–1-AP).

After 2 10-min washes with 1 × TBST, membranes were incubated with appropriate IRDye secondary antibodies at room temperature on slow shaker for 1.5 h. The membranes were washed in 1 × TBST for 5 min prior to band detection using the LI-COR Odyssey Infrared Imaging System. Protein band intensities were quantified using Image J (NIH, Bethesda, MD). Revert™ 700 total protein membrane staining (LI-COR) or silver stain (BIO-RAD) was used as an internal control for target normalization according to manufacturer's instructions. Revert™ 700 total protein membrane staining was also used for protein foot printing.

Data visualization, PPI analysis, and pathway identification

Venn diagrams were generated using VENNY platform (v2.1) [47]. Heatmaps were generated using Heatmapper [48]. Average linkage cluster and Euclidean distance measurement was applied to rows and columns of all heatmaps. Principal component analysis (PCA) plot was generated using ClustVis [49]. Protein–protein interaction (PPI) network was visualized, and functional enrichment analysis was determined using STRING (https://string-db.org/) database V11.5 [50]. Pathways were identified using WEB-based GEne SeT AnaLysis Toolkit 2019 (WebGestalt) (www.webgestalt.org) [51]. The parameters used in WebGestalt were over-representation analysis (ORA) of gene symbols

GP1BA, CD31, CAPN1, HSPB1, and ANXA5 within the cancer Wikipathway functional database referenced to the genome.

BEV labeling, internalization, and MTT assays

Pooled BEVs (100 µg) were concentrated using amicon ultra-0.5 centrifugal filter units (Millipore Sigma) by centrifuging at 14,000 g for 5 min to remove excess PBS. Resulting volumes were filled to 100 µl to label BEVs with green, fluorescent dye (SYTO™ RNASelect™ stain for RNA—Invitrogen™) according to the manufacturer's instructions. After labeling, unincorporated dye was removed using exosome spin columns (MW3000—Invitrogen™) according to the manufacturer's instructions. PBS mixed with dye was used as negative control. 5000 cells/100 µl of luminal A MCF7 and basaloid MDA-MB-231 breast cancer cells seeded in each well (5 wells per 3 independent experiments) of a 96-well plate were treated with labeled BEVs at 100 µg/mL and incubated for 24 and 48 h (hours). 100 µg/mL of BEVs was used based on preliminary dose–response experiments that showed it was within the linear range of the curve compared to lower (low response) and higher concentrations (saturating response) of BEVs (Supplementary Fig. 4). Images of cells with internalized fluorescently labeled BEVs were obtained after 24 h using a Lionheart FX automated microscope at 10x. Cell viability was assessed using an MTT (3-[4,5-dimethylthiazol-2-yl]-2,5 diphenyl tetrazolium bromide) assay, each well was treated with 20 µl of MTT reagent and incubated at 37 °C for 3 h. After 3 h, 100 µl of MTT solvent was added to each well and the plate was covered from light while shaking for 30 min. The absorbance of solubilized MTT reagent was measured using a spectrophotometer at 590 nm.

Statistical analysis

The log10 values of spectral counts and precursor abundances of all proteins were compared using a one-way ANOVA Šídák's multiple comparisons test. The mean of each protein for R and NR were compared. Differences were considered significant with p-adjusted values < 0.05. For validation experiments, samples from individual patients were pooled as described in the legend of Fig. 6A or pooled as R ($n = 6$) versus NR ($n = 9$) in two independent experiments. For viability experiments, error bars represent standard error of the mean (SEM) of three replicate wells. Experiments were repeated at least twice with similar results. Two-tailed unpaired t-test with Welch's correction was used to determine differences between groups in all figures, unless noted otherwise. Error bars represent SEM for all graphs unless noted otherwise. GraphPad Prism (v9.2.0) was used to plot all graphs and perform all statistical analyses.

Results

PPLC separates BEVs from major contaminants

Here we evaluated the utility of PPLC (Fig. 1) for isolating BEVs that are free of major contaminants. PPLC was used to separate blood plasma and UV–Visible spectroscopy (UV-VIS) analytics was applied to determine EV size, concentration, and to retrieve information on analytes in subpopulations. As shown in Fig. 2a, the PPLC separation profile shows four distinct peaks *i.e.,* P1, P2a-2c, P3, P4. Western blot analysis was used to distinguish EVs and lipoprotein markers in the individual fractions (Fig. 2b, Top). Silver staining showed the protein footprint of the different fractions (Fig. 2b, Bottom). Integration of the western blot and silver stain results demonstrate that the first peak (Fig. 2a, P1 blue bar) contains EVs depleted by > 90% of lipoproteins (ApoA1) and albumin (ALB). The first few fractions of P1 (Fig. 2b, F47-F60) are the most enriched, as indicated by the EV marker CD9 and absence of detectable lipoprotein marker (ApoA1) and albumin (ALB). The ascending part of P2 (P2a) contains the most of ApoA1 protein with no CD9 (Fig. 2b), indicating strong presence of lipoproteins, perhaps from the largest type: chylomicron (80–1200 nm [52]), very-low-density lipoproteins (VLDL, 30–90 nm [52]), and low-density lipoproteins (LDL, 18–25 nm [52]), as expected from a size-exclusion chromatography (SEC) based purification. The top part of P2 (P2b) contains the least diverse proteins with thick banding at ~ 66 KDa and no ApoA1 or CD9 consistent with ALB enrichment. Interestingly, a second ApoA1-containing population appeared in the descending part of P2 (P2c), indicating presence of high-density lipoproteins (HDL), which are the smallest lipoproteins (5–20 nm [52]). P3 contained a unique and diverse protein profile that may reflect a novel class of membraneless condensates (MCs), with size not larger than a few nanometers. P4 contained little or no detectable proteins indicating the enrichment in sub-nanometer molecules such as sugars, nucleotides, amino acids, vitamins, minerals and/or salts. This fraction was not analyzed further.

The integrative western blot and silver stain analyses corroborates the 3D (Fig. 2c) and individual spectral (Fig. 2d) data, where P1 exhibits a typical EV profile with a shoulder in the turbidity range that is well detected even within P2 (Fig. 2c, d). As shown in Fig. 2d, P2a showed a unique sharp absorbance peak at ~ 415 nm. P2b is distinguished with a 443 nm peak, absent in P2c. P3 on the other hand sharply blue-shifted to 275 nm. This analysis was confirmed by the negative-stain TEM visualization of the fractions (Fig. 2e) that showed P1 had highly pure 100–400 nm vesicles. P2a contained a mixture of smaller vesicles 30–150 nm comprising VLDL (typical range 30–90 nm). P2b showed pure

aggregates of dense particles with a primary particle size of 18–25 nm, typical size range for LDL. P2c also shows dense particles with relatively smaller sizes (5–20 nm), a typical size range for HDL. P3 contained aggregates of MCs (Fig. 2e). Altogether, our data demonstrate that PPLC can efficiently separate and characterize complex biological samples such as blood plasma in real-time, retrieve subpopulations of EVs of interest, such as CD9 + EVs.

Comparison of the physicochemical properties of BEVs from R and NR breast cancer patients

Using the PPLC workflow (Fig. 1), we separated blood plasma from 7 R and 10 NR breast cancer patients. The EV fractions (P1) shown in Fig. 3a (top for R and bottom for NR) were collected. PPLC analytics was used to determine BEV size and concentration. The sizes (98.6 to 102.3 nm) of BEVs from R and NR are not significantly different (Fig. 3b). In contrast, BEV concentration per mL of blood plasma was significantly lower in R compared to NR (Fig. 3c). Additionally, the electrostatic properties (measured as ζ potential) of BEV membrane show that R BEVs bear subtle negative charge (-27.8 ± 6.1 mV) that is significantly different from the ζ-potential (-35.3 ± 7.4 mV) of NR BEVs (Fig. 3d). There is no difference in the total protein content of R versus NR BEVs (Fig. 3e) and the protein footprint between R and NR BEVs was similar irrespective of whether equal protein (25 µg) or equal particle number (4E + 09) was used (Fig. 3f). Western blot analysis shows that some R and NR BEVs contain CD63 and CD81 EV markers but negative for endoplasmic reticulum marker calnexin (Fig. 3g, Supplementary Fig. 1). Additionally, negative-stain TEM coupled with CD9 immuno-labelling of R and NR BEVs validates that the BEVs are similar and are CD9 reactive (Fig. 3h). Together, these data show that despite individual variabilities, NR patient blood plasma contain more BEVs (Fig. 3c) that bear more negative surface charge (Fig. 3d).

No significant differences in BEV size, concentration and ζ-potential based on HER2, ER, PR receptor status, lymph node involvement, and molecular subtype grouping

Patients who are ER + ($n=9$), PR + ($n=8$), or HER2 + ($n=7$) have similar BEV size, concentration and ζ-potential compared to those who are ER- ($n=8$), PR- ($n=9$), and HER2- ($n=10$) (Fig. 4a–c). No significant difference in BEV size, concentration and ζ-potential were detected between triple negative breast cancer (TNBC) patients ($n=5$) and 12 patients designated as other (Fig. 4d). We also did not observe statistically significant difference in BEV size, concentration and ζ-potential between patients who were lymph node positive or negative prior to NAC (Fig. 4e). Grouping

the patients according to tumor molecular subtype did not provide significant differences in BEV size, concentration, and ζ-potential (Fig. 4f).

Global protein profiling of BEVs from R and NR

Global protein profiling of BEVs was conducted using quantitative LC–MS/MS. Each patient sample was subjected to LC–MS/MS twice for technical replicates (R = 14; NR = 20). Relative protein quantification between R and NR were performed using spectral counts (SpC), which compares the number of MS/MS spectra assigned to each protein. Using log10 values of SpC for all proteins with a sum SpC ≥ 5 across all samples ($n=34$) and SpC ≥ 2 for at least one sample out of all samples, we identified 907 proteins (Fig. 5a, Supplementary Table I). The percentage of proteins detected exclusively for R and NR were 0.7% (6) and 10.8% (98) respectively (Fig. 5b). We also found 88.5% (803) of proteins to be in common between R and NR (Fig. 5b). A comparison of R and NR BEV proteins to the top-100 Exocarta (http://www.exocarta.org) and Vesiclepedia (www.microvesicles.org) EV proteins, revealed 1 NR protein exclusively in the Exocarta list, 5 NR proteins in the Exocarta and Vesiclepedia list, 11 of R and NR proteins in the Exocarta list, 15 of R and NR proteins in the Vesiclepedia list and 52 of R and NR proteins both in the Exocarta and Vesiclepedia list (Fig. 5c). Therefore, more than 50% of the top-100 Exocarta and Vesiclepedia EV proteins were identified in R and NR BEVs. Common EV markers CD9, HSP90AB1, HSPA8, YWHAZ, and ANXA5 were among those identified in our study (Supplementary Table II). To identify differentially enriched proteins in the BEVs, we averaged the log10 values of spectral counts (SpC) of the technical replicates for all 907 proteins to further analyze the samples as biological replicates (R = 7; NR = 10) and performed the stringent Šídák's multiple comparisons test. To limit counting bias associated with proteins falsely discovered by the SpC method, we used the area under the curve (AUC) method that accounts for peptide precursor abundances. Hence, we averaged the log10 values of precursor abundances for all 907 proteins to perform a Šídák's multiple comparisons test. The SpC method yielded 60 differentially enriched proteins with P-adjusted values < 0.05 (Fig. 5d, Supplementary Fig. 2a, Table 2), and the AUC method yielded 19 differentially enriched proteins with P-adjusted values < 0.05 (Fig. 5e, Supplementary Fig. 2b, Table 3). While the 19 proteins identified via the AUC method clustered the NR from the R group (Fig. 5e), a principal component analysis (PCA) plot revealed an imperfect clustering with a responding patient overlapping with the NR group (Fig. 5f). Therefore, to further narrow down a list of proteins that can differentiate R from NR breast cancer patients, we compared the SpC (60) and AUC (19) protein list using a 2-way Venn diagram and identified 8 proteins
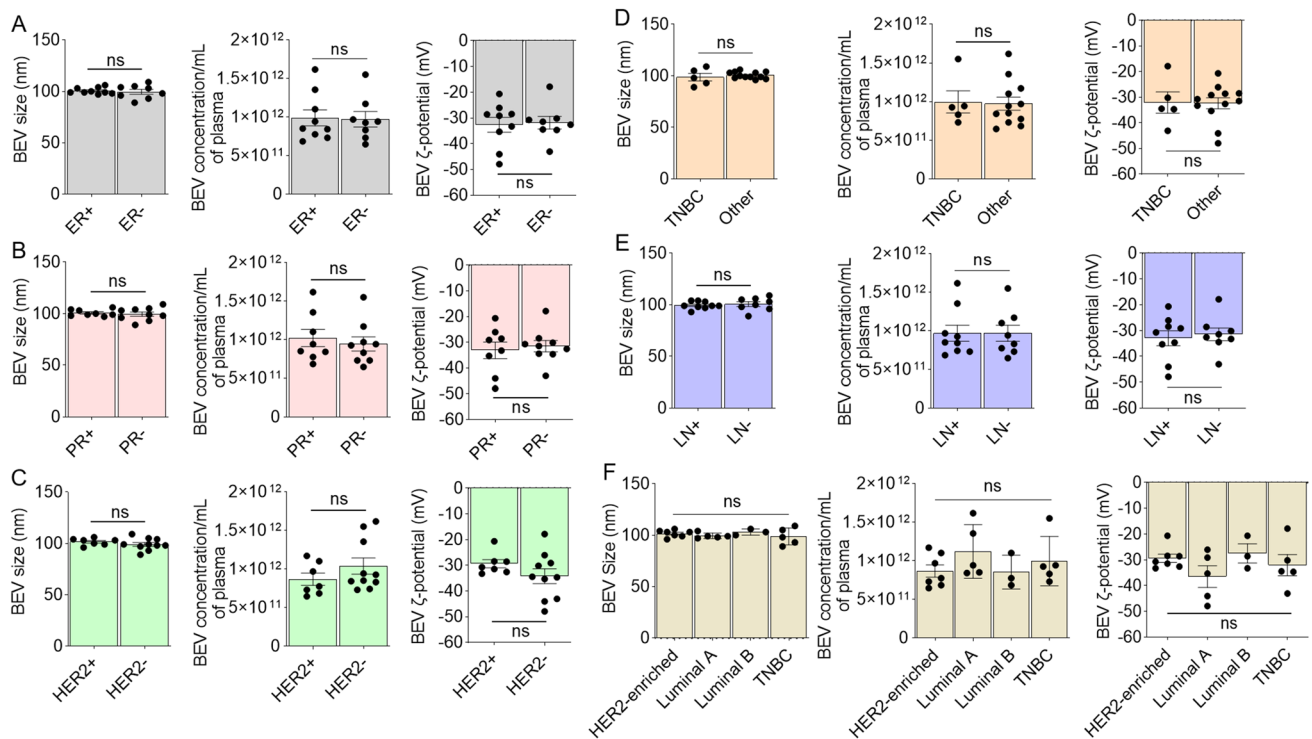
Fig. 4 Comparison of BEV size, concentration and ζ-potential based on HER2, ER, PR, receptor status, lymph node involvement, and molecular subtype grouping. BEV size, concentration and ζ-potential comparison between breast cancer patients that are: **A** ER+ ($n=9$) and ER- ($n=8$); **B** PR+ ($n=8$) and PR- ($n=9$); **C** HER2+ ($n=7$) and HER2- ($n=10$); **D** triple negative (TNBC) ($n=5$) and other ($n=12$); **E** lymph node (LN)+ ($n=9$) and LN- ($n=8$) prior to NAC; **F** HER2+ ($n=7$), Luminal A ($n=5$), Luminal B ($n=3$) and TNBC ($n=5$). *Unpaired t-test with Welch's correction used to determine differences between groups*

(GP1BA (CD42b), PECAM-1 (CD31), CAPN1, HSPB1 (HSP27), ANXA5, RAB11A, SLC2A3, and G6PD) to be unique to both lists (Fig. 5g). Hierarchical clustering heatmap of the 8 proteins showed that R and NR BEV proteomes clustered separately (Fig. 5h). This was further confirmed with a PCA plot showing that R and NR BEVs are separated by the biplot of PC1 and PC2 representing a nearly perfect clustering (Fig. 5i). The enrichment levels of the 8 proteins are presented in Supplementary Figs. 3a–b. These data suggest that R and NR BEVs undergo alterations in their protein composition.

Validation of the eight proteins significantly enriched in BEVs from NR

The levels of the 8 proteins identified by proteomic analysis to be enriched in NR BEVs were analyzed by western blot for validation. The analysis confirmed the presence of GP1BA (CD42b), PECAM-1 (CD31), CAPN1, HSPB1 (HSP27), and ANXA5 (Fig. 6a). However, RAB11A, SLC2A3, and G6PD were not detected. Quantitatively, the relative band intensities of the proteins were significantly higher in NR compared to R BEVs (Fig. 6b). These results corroborate the proteomics data (Supplementary Figs. 3a–b)

and strongly suggests that GP1BA (CD42b), PECAM-1 (CD31), CAPN1, HSPB1 (HSP27), and ANXA5 are differentially present proteins (DEPs) in BEVs from NR breast cancer patients.

Functional and pathway enrichment analysis of identified BEV proteins from NR

STRING [50] database was used to visualize protein–protein interaction (PPI) networks and determine functional enrichment of GP1BA (CD42b), PECAM-1 (CD31), CAPN1, HSPB1 (HSP27), and ANXA5 (Fig. 6c). Functional analysis of the PPI network revealed wound healing (biological process), extracellular vesicle and external side of plasma membrane (cellular component) gene ontology (GO) terms to be significantly (*PPI enrichment p-value = 0.000921*) enriched (Fig. 6c). Pathway analysis using WebGestalts cancer Wikipathways functional database revealed CAPN1 to be within the gene set of the Integrin-mediated cell adhesion pathway (Fig. 6d). HSPB1 was found to be within the gene set of the MAPK signaling pathway and significantly (*p-value = 0.05*) enriched within the gene set of the ATM signaling network in development and disease (Fig. 6d).
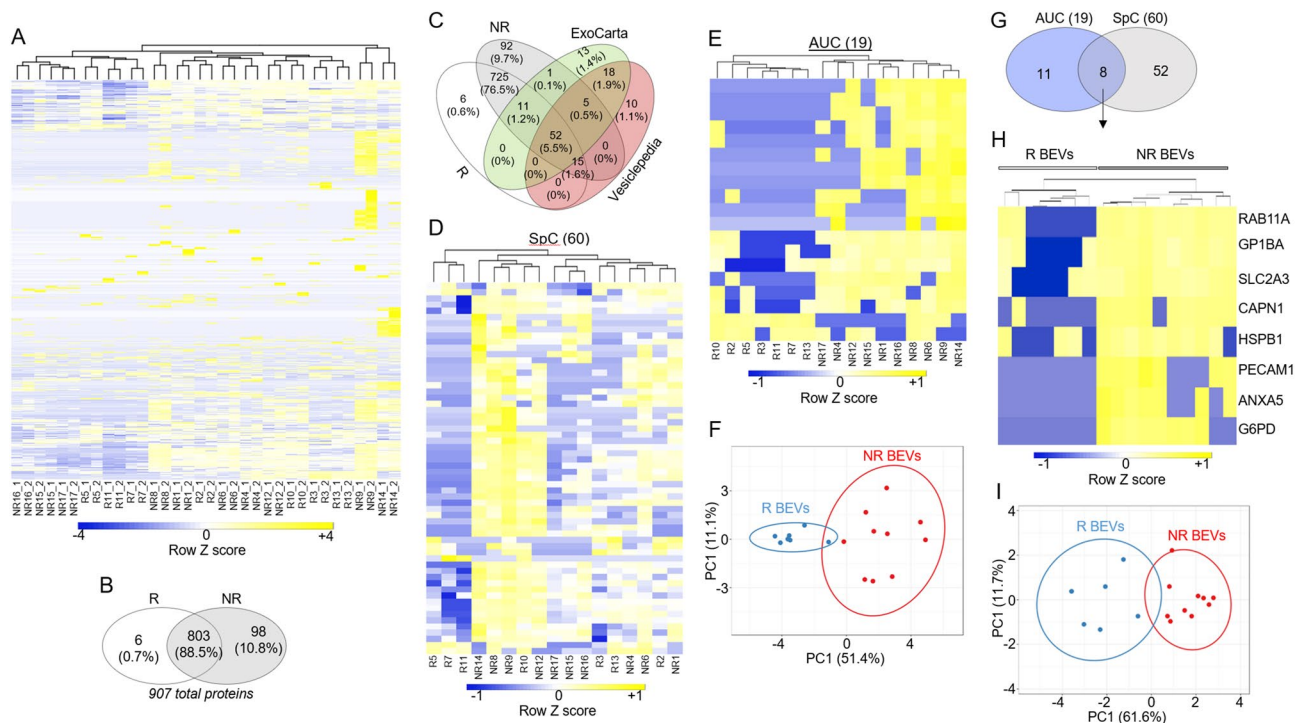
Fig. 5 Stringent proteomic analysis reveals 8 proteins significantly enriched in NR BEVs. **A** Heatmap of total proteins identified (907) in technical replicates of BEV samples (R = 14, NR = 20). **B** 2-way Venn diagram of proteins in (A) with spectral counts (SpC) ≥ 2 in at least one patient of each group. **C** 4-way Venn diagram comparing proteins in (A) to top-100 EV proteins of Exocarta and Vesiclepedia repository. **D** Heatmap of averaged technical replicate log10 values of SpC for proteins in (A) with a p-adjusted value < 0.05 measured by a Šídák's multiple comparison test. **E** Heatmap of averaged technical replicate log10 values of precursor abundances (AUC) for proteins in (A) with a p-adjusted value < 0.05 measured by a Šídák's multiple comparison test. **F** principal component analysis (PCA) plot depicting imperfect clustering of R and NR patients using the 19 proteins identified by the AUC method. **G** 2-way Venn diagram of 60 and 19 proteins identified via SpC and AUC, respectively. **H** Heatmap of 8 proteins common to SpC (60) and AUC (19). **I** PCA plot depicting clustering of R and NR patients using the identified 8 proteins.

Cancer cells internalize BEVs from R and NR

To investigate differential biological activity of BEVs from R and NR patients, we evaluated the ability of the luminal MCF-7 and basaloid MDA-MB-231 breast cancer cell lines to internalize BEVs derived from the patient cohort. Pooled BEVs from R and NR patients were labeled with SYTO™ green stain as previously described [5]. Cells treated with SYTO™ labelled PBS were used as negative control. Results from fluorescence microscopy show the absence of detectable fluorescence in cells after 24 h (hours) of being treated with PBS containing SYTO™ green stain (Fig. 7a, b). Whereas positive fluorescence signals in cultured MCF7 (Fig. 7a) and MDA-MB 231 (Fig. 7b) cells support tumor cell uptake of BEVs obtained from both R and NR patients. While we observed BEV uptake by breast cancer cells, differential uptake was not evaluated due to limited samples.

BEVs from R and NR increase metabolic activity of breast cancer cells

Having confirmed that breast cancer cells are able to internalize BEVs from both R and NR, we next investigated the effect of BEVs on breast cancer cell metabolic activity. As shown in Fig. 7c, treatment of MCF7 cells with BEVs from R and NR showed a significant increase in MTT conversion to formazan at 24 and 48 h over PBS control. Notably, this effect was significantly greater with BEVs from NR patients 48 h post treatment (Fig. 7c). To validate this effect, MDA-MB 231 cells treated with BEVs from R and NR were also analyzed for MTT activity. The result showed that unlike the response of MCF7 cells, only BEVs from NR significantly increased MTT conversion in MDA-MB 231 cells post treatment both at 24 h and 48 h (Fig. 7d). These data shows that BEVs released by both R and NR can increase the conversion of MTT to formazan suggesting an increase in mitochondrial activity (metabolic) and/or cell proliferation (mitogenic)

Table 2 Averaged log10 values of spectral counts (SpC) of the technical replicates for the total 907 proteins yielded 60 differentially enriched proteins ordered by p-adjusted value < 0.0001**** to < 0.05* using the stringent Šídák's multiple comparisons test.

Protein name	
FLNA****	GC**
MYH9****	TAGLN2**
FERMT3****	SSC5D**
ITGB3****	CAPZB**
F13A1****	ACTR2**
ITGA2B****	ALAD**
F5****	UBA1**
SLC4A1****	GANAB**
TUBB1****	GRB2**
MMRN1****	HSP90AB1**
ILK****	ANXA5**
ENO1****	PECAM1**
VASP****	GAPDH*
CLTC****	RAP1B*
YWHAH****	PNP*
C9****	ARPC2*
PDLIM1****	ARPC1B*
GP1BA****	BIN2*
LIMS1****	CA2*
HSPB1****	HK1*
G6PD****	TALDO1*
TLN1***	LBP*
WDR1***	PARK7*
PGK1***	ARPC3*
HSP90AA1***	TUBB*
PRDX6***	F13B*
LDHB***	SLC2A3*
RAB11A***	ATP5A1*
CAPN1***	ALOX12*
FCGBP**	ANPEP*

Table 3 Area under the curve (AUC) proteomic analysis performed by averaging the log10 values of precursor abundances of the total proteins (907) yielded 19 differentially enriched proteins ordered by p-adjusted value < 0.0001**** to < 0.05* using the stringent Šídák's multiple comparisons test.

Protein name
S100A4****
RAB11A***
SLC2A3***
UGP2***
HSPB1**
CAPN1**
LDHA**
ANXA5**
ALMS1**
GP1BA*
G6PD*
PECAM1*
CAPZA2*
MYL9*
MYL6*
EEF1A1*
STX11*
OR6B1*
TPT1*

and that the effects of BEVs may differ by tumor cell lines or tumor subtypes.

Discussion

The interrogation of EVs as mediators of intercellular/interorgan communication is of increasing interest for their role in health and disease and potential clinical utility. The accessibility of EVs in body fluids, such as urine, saliva, semen, breast milk, amniotic fluid, and blood, make EVs a highly attractive source for novel diagnostic and predictive biomarkers, as well as for the discovery of novel therapeutic targets. Under normal and some harsh handling of EV samples, EV-associated biomolecular cargos are highly stable over time [13]. This stability makes EVs highly informative biomolecules when compared to other components of liquid biopsies, such as less stable circulating tumor cells.

Our primary objective was to characterize and establish the preanalytical conditions for isolating pure EVs from blood plasma prior to biomarker identification. It is important to note that while this study was conducted with blood plasma from R and NR breast cancer patients, it is reasonable to assume that the findings and principles are generalizable to blood plasma EV studies and the EV isolation and characterization strategy applicable to other body fluids [1].

Our study supports the use of PPLC to improve the isolation of BEVs and separate them from contaminants, such as lipoproteins, albumin, and MCs. Lipoproteins and albumin are the most abundant circulating proteins in blood plasma [61, 62]. Their abundance in plasma and non-specific binding properties are well recognized challenges in protein-based biomarker discovery, particularly for detecting moderate and low abundance proteins. While methods for depleting lipoproteins and albumin from samples have been developed [63, 64] including delipidation, these methods (i) involve the use of organic solvents that denature proteins, (ii) decrease specificity in proteomic studies (immunoprecipitation) [65], and/or (iii) reduce the recovery of membrane-associated proteins such as those present on EVs. Hence, PPLC has the potential to address these shortcomings as described in Figs. 2 and 3.

It has been reported that breast cancer patients prior to receiving NAC contain significantly elevated levels of EVs in their blood serum compared to healthy patients [66]. In addition, elevated levels of blood plasma EVs have been associated with therapy failure and disease progression in breast cancer patients undergoing NAC [67]. However, the

Fig. 6 Validation and potential biological functions of 5 differentially present proteins (DPPs) in NR BEVs. **A** Western blot validation of 5 DPPs using total protein as loading control. R1, 2, 3 each are a pool of 2 different patients (R = 6). NR 1, 2, 3 each are a pool of 3 different patients (NR = 9). **B** Protein band intensity of 5 DPPs normalized to total protein from three independent experiments (equal protein or equal EV number loaded). **C** STRING protein interaction network analysis of 5 DPPs. **D** HSPB1 and CAPN1 gleaned via WebGestalt WikiPathway cancer database. **E** HSPB1 linkage to chemoresistance. *Unpaired t-test with Welch's correction was used to determine differences between groups. *p < 0.05. **p < 0.01*
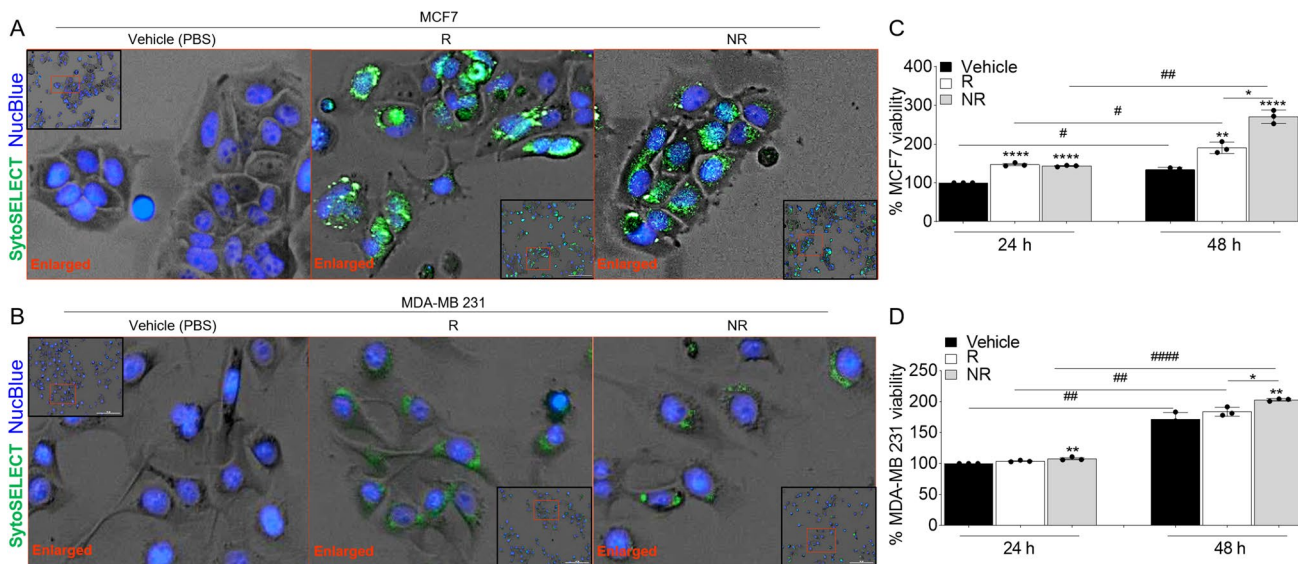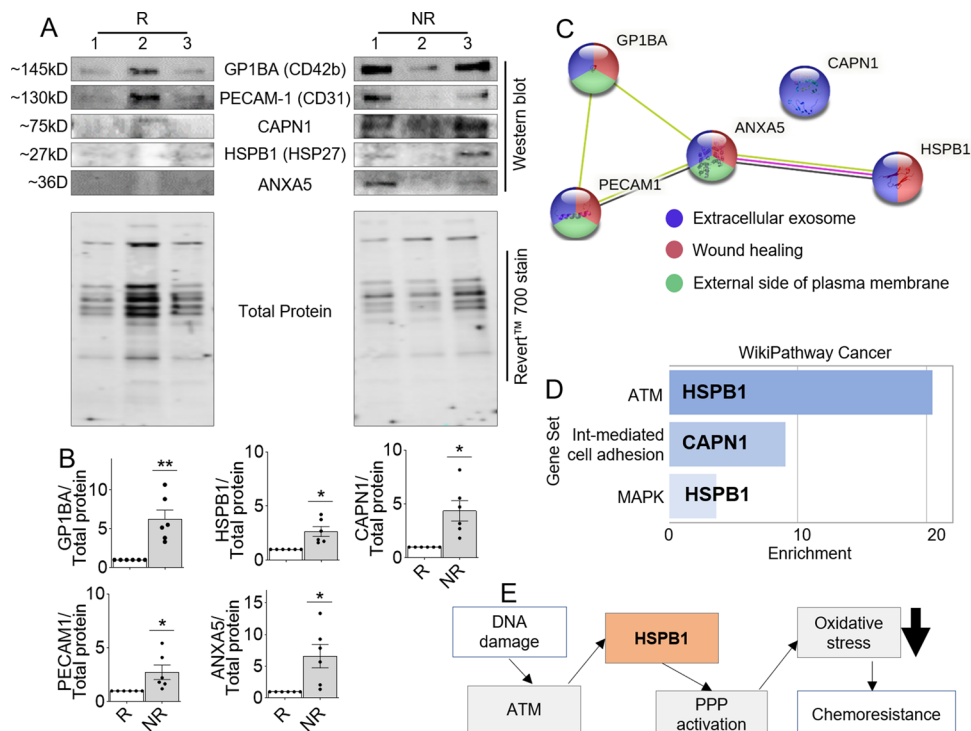
Fig. 7 Breast cancer cells internalize R and NR BEVs and the internalized BEVs promote metabolic activity of breast cancer cells. **A–B** Images of (**A**) MCF-7 cells and (**B**) MDA-MB 231 cells incubated with SYTO™ RNASelect™ stained BEVs (100 µg) for 24 h (h). DAPI is in blue and SYTO™ RNASelect™, which stained BEV RNA is in green. Fluorescence images were manually obtained with Lionheart FX automated microscope at 10X. The inset is the zoomed-out image. Red rectangles correspond to the enlarged area. Scale bar: 50 µm. **C–D** MTT assay for metabolic activity of (**C**) MCF-7 and (**D**) MDA-MB 231 cells following 24–48 h incubation with 100 µg/ml of BEVs. *Ordinary one-way ANOVA (Brown-Forsythe and Bartlett's tests, with Šídák's multiple comparisons test) was used to determine the statistical significance within the group. Binary Student's t-test (Welch's correction) was used between groups and time points. *p < 0.0113, ****p < 0.0001, **p < 0.004, #p < 0.0112, ##p < 0.0056, ####p < 0.0001*

composition of these cancer derived blood EVs and their ability to alter recipient cellular behavior is unknown. Hence, our longer-term objective is to determine the utility of BEV-associated proteins to study patient response to cancer treatment. Using a small discovery cohort, we observed striking differences in the physicochemical properties of

BEVs from patients who responded (R) to NAC and those that did not (NR) for the treatment of locally advanced breast cancer.

While the differences in the proteome of BEVs may be used to differentiate NR patients, the significantly elevated concentration and more negative zeta potential (surface charge) of NR BEVs compared to R BEVs may influence different biological processes associated with BEVs, such as cellular uptake and cytotoxicity [68]. Under physiological conditions, cells are negatively charged so it may be likely that negatively charged BEVs may have an increased tendency to repel cells. Hence, a plausible scenario may be that NR patients with more BEVs which are highly negatively charged may trap NAC and prevent it from reaching the patient's cancer cells resulting in chemoresistance.

Using LC–MS/MS, a set of proteins were identified that were differentially enriched in NR compared to R supporting the potential utility of our approach to detect circulating EV biomarkers associated with patient response. The proteomics data highlights the importance of BEV cargo and uncovers the potential for future research into the mechanisms of chemoresistance in breast cancer patient cohort. A closer look at the function of HSPB1 within the gene set of the ATM signaling network in disease (Fig. 6d) revealed its direct link in activating the pentose phosphate pathway (PPP) to inhibit oxidative stress. The gene set signaling network suggests that upon DNA damage, ATM is activated which leads to HSPB1 activation, followed by PPP activation to inhibit oxidative stress. Chemotherapy causes DNA damage [53] and oxidative stress [54] to slow cancer cell cycle progression that eventually leads to activation of cell death [55]. Interestingly, HSPB1 has been shown to be overexpressed in many types of human cancers, including breast cancer and a poor prognostic for patient survival [56–58]. In addition, overexpression of HSPB1 causes resistance to doxorubicin-induced apoptosis in breast cancer cells [59] and chemotherapy in breast cancer patients [60]. However, the mechanisms for the resistance to chemotherapy is not understood. Here, we show that HSPB1 is enriched in BEVs of NR breast cancer patients and propose a possible HSPB1-mediated mechanism of chemoresistance by inhibiting oxidative stress upon chemotherapy-induced DNA damage (Fig. 6e). Also discovered was the increase in metabolic activity of breast cancer cells when treated with NR BEVs. The biological implication of this result hints at the NR BEVs counteracting the expected effects of NAC on NR patients breast cancer cells. However, these implications require further investigation.

Conclusion

The study of BEV-associated proteins in cancer and other diseases and their potential clinical utility requires analyte validity and reproducibility of results. Here, we used PPLC to isolate near-pure BEVs from a small breast cancer patient cohort and showed that they retained function for experimental studies and demonstrated their utility to identify differentially present BEV proteins related to patient treatment response. Future efforts will be directed at validating our results in a larger sample size and in functionally characterizing BEV protein effects on tumor growth in model systems.

Limitations of the study and interpretation

The patient blood plasma samples used in this study were obtained using blood collection tubes containing the anticoagulant EDTA and used within one year of storage at − 80 °C after a single freeze thaw. Because tube type and different anticoagulants can alter plasma chemistry [69], fractionation methods for BEVs may require optimization based on tube type. Although we previously showed that storage condition can affect the biologic activity of semen derived EVs [13], the effect of time of collection and storage condition was not studied, and this is as a limitation of this study.

Moreover, our study included a single hospital, Stony Brook University Renaissance School of Medicine Hospital with a limited patient cohort and sample size. Thus, our results require validation with a larger patient population from different geographic locations and diverse backgrounds. Our study also included only cancer patients. Inclusion of healthy donors may improve the predictive and statistical power of our results. Finally, we only analyzed BEVs in this study and did not relate our findings to other plasma analytes (lipoproteins, albumin, and MCs) or blood serum [36, 70] that may share or add additional informative biomarkers.

Data availability Spectral counts and precursor abundances dataset with peptide spectrum match annotations are attached to this manuscript as additional files.

Declarations

Conflicts of interest The authors declare that they have no competing interests.

Ethical approval This study was conducted according to university regulations approved by Stony Brook University Institutional Review Boards (IRB # 860033).

Consent to participate Individuals who met the inclusion and exhibit none of the exclusion criteria and who gave written informed consent were included in the study.

References

1. Kaddour H, Lyu Y, Shouman N, Mohan M, Okeoma CM (2020) Development of novel high-resolution size-guided turbidimetry-enabled particle purification liquid chromatography (PPLC): extracellular vesicles and membraneless condensates in focus. Int J Mol Sci. 21(15):5361

2. Kaddour H, Lyu Y, Welch JL, Paromov V, Mandape SN, Sakhare SS, Pandhare J, Stapleton JT, Pratap S, Dash C et al (2020) Proteomics profiling of autologous blood and semen exosomes from HIV-infected and uninfected individuals reveals compositional and functional variabilities. Mol Cell Proteom. 19(1):78–100

3. Kaddour H, Panzner TD, Welch JL, Shouman N, Mohan M, Stapleton JT, Okeoma CM (2020) Electrostatic surface properties of blood and semen extracellular vesicles: implications of sialylation and HIV-induced changes on EV internalization. Viruses. 12(10):1117

4. Lyu Y, Kaddour H, Kopcho S, Panzner TD, Shouman N, Kim EY, Martinson J, McKay H, Martinez-Maza O, Margolick JB et al (2019) Human Immunodeficiency Virus (HIV) infection and use of illicit substances promote secretion of semen exosomes that enhance monocyte adhesion and induce actin reorganization and chemotactic migration. Cells. 8(9):1027

5. Lyu Y, Kopcho S, Mohan M, Okeoma CM (2020) long-term low-dose delta-9-tetrahydrocannbinol (THC) administration to simian immunodeficiency virus (SIV) infected rhesus macaques stimulates the release of bioactive blood extracellular vesicles

6. Madison MN, Jones PH, Okeoma CM (2015) Exosomes in human semen restrict HIV-1 transmission by vaginal cells and block intravaginal replication of LP-BM5 murine AIDS virus complex. Virology. 482:189–201

7. Madison MN, Okeoma CM (2015) Exosomes: implications in HIV-1 pathogenesis. Viruses 7(7):4093–4118

8. Madison MN, Roller RJ, Okeoma CM (2014) Human semen contains exosomes with potent anti-HIV-1 activity. Retrovirology 11:102

9. Madison MN, Welch JL, Okeoma CM (2017) Isolation of exosomes from semen for in vitro uptake and HIV-1 infection assays. Bio-Protoc. 7(7): e2216

10. Welch JL, Kaddour H, Schlievert PM, Stapleton JT, Okeoma CM (2018). Semen Exosomes Promote Transcriptional Silencing of HIV-1 by Disrupting NF-κB/Sp1/Tat Circuitry. J Virol. 92(21):e00731-18

11. Welch JL, Kaddour H, Winchester L, Fletcher CV, Stapleton JT, Okeoma CM (2020) Semen extracellular vesicles from HIV-1-infected individuals inhibit HIV-1 replication in vitro, and extracellular vesicles carry antiretroviral drugs in vivo. J Acquir Immune Defic Syndr. 83(1):90–98

12. Welch JL, Kaufman TM, Stapleton JT, Okeoma CM (2020) Semen exosomes inhibit HIV infection and HIV-induced pro-inflammatory cytokine production independent of the activation state of primary lymphocytes. FEBS Lett. 594(4):695–709

13. Welch JL, Madison MN, Margolick JB, Galvin S, Gupta P, Martinez-Maza O, Dash C, Okeoma CM (2017) Effect of prolonged freezing of semen on exosome recovery and biologic activity. Sci Rep. 7:45034

14. Welch JL, Stapleton JT, Okeoma CM (2019) Vehicles of intercellular communication: exosomes and HIV-1. J Gen Virol. 100(3):350-366

15. Anfossi S, Babayan A, Pantel K, Calin GA (2018) Clinical utility of circulating non-coding RNAs—an update. Nat Rev Clin Oncol 15(9):541–563

16. Batagov AO, Kurochkin IV (2013) Exosomes secreted by human cells transport largely mRNA fragments that are enriched in the 3′-untranslated regions. Biol Direct 8:12

17. Jin Y, Chen K, Wang Z, Wang Y, Liu J, Lin L, Shao Y, Gao L, Yin H, Cui C et al (2016) DNA in serum extracellular vesicles is stable under different storage conditions. BMC Cancer 16(1):753

18. Raposo G, Stoorvogel W (2013) Extracellular vesicles: exosomes, microvesicles, and friends. J Cell Biol 200(4):373–383

19. Vojtech L, Woo S, Hughes S, Levy C, Ballweber L, Sauteraud RP, Strobl J, Westerberg K, Gottardo R, Tewari M et al (2014) Exosomes in human semen carry a distinctive repertoire of small non-coding RNAs with potential regulatory functions. Nucleic Acids Res 42(11):7290–7304

20. Lee H, Castro CM (2019) Thermophoretically enriched detection. Nat Biomed Eng 3(3):163–164

21. Balaj L, Lessard R, Dai L, Cho YJ, Pomeroy SL, Breakefield XO, Skog J (2011) Tumour microvesicles contain retrotransposon elements and amplified oncogene sequences. Nat Commun 2:180

22. Liu C, Xu X, Li B, Situ B, Pan W, Hu Y, An T, Yao S, Zheng L (2018) Single-Exosome-counting immunoassays for cancer diagnostics. Nano Lett 18(7):4226–4232

23. Zhang L, Wang H, Zhao G, Li N, Wang X, Li Y, Jia Y, Qiao X (2021) Anti-Tim4 grafting strongly hydrophilic metal-organic frameworks immunoaffinity flake for high-efficiency capture and separation of exosomes. Anal Chem 93(16):6534–6543

24. Yang L, Yin X, An B, Li F (2021) Precise capture and direct quantification of tumor exosomes via a highly efficient dual-aptamer

recognition-assisted ratiometric immobilization-free electrochemical strategy. Anal Chem 93(3):1709–1716

25. Huang M, Yang J, Wang T, Song J, Xia J, Wu L, Wang W, Wu Q, Zhu Z, Song Y et al (2020) Homogeneous, low-volume, efficient, and sensitive quantitation of circulating exosomal PD-L1 for cancer diagnosis and immunotherapy response prediction. Angew Chem Int Ed Engl 59(12):4800–4805

26. Zhu L, Xu Y, Wei X, Lin H, Huang M, Lin B, Song Y, Yang C (2021) Coupling aptamer-based protein tagging with metabolic glycan labeling for in situ visualization and biological function study of exosomal protein-specific glycosylation. Angew Chem Int Ed Engl 60(33):18111–18115

27. Zhang P, Zhou X, Zeng Y (2019) Multiplexed immunophenotyping of circulating exosomes on nano-engineered ExoProfile chip towards early diagnosis of cancer. Chem Sci 10(21):5495–5504

28. György B, Pálóczi K, Kovács A, Barabás E, Bekő G, Várnai K, Pállinger É, Szabó-Taylor K, Szabó TG, Kiss AA et al (2014) Improved circulating microparticle analysis in acid-citrate dextrose (ACD) anticoagulant tube. Thromb Res 133(2):285–292

29. Cvjetkovic A, Lötvall J, Lässer C (2014) The influence of rotor type and centrifugation time on the yield and purity of extracellular vesicles. J Extracell Vesicles. 3.

30. Ding L, Liu LE, He L, Effah CY, Yang R, Ouyang D, Jian N, Liu X, Wu Y, Qu L (2021) Magnetic-Nanowaxberry-Based simultaneous detection of exosome and exosomal proteins for the intelligent diagnosis of cancer. Anal Chem. 93, 45, 15200–15208

31. Perales S, Torres C, Jimenez-Luna C, Prados J, Martinez-Galan J, Sanchez-Manas JM, Caba O (2021) Liquid biopsy approach to pancreatic cancer. World J Gastrointest Oncol 13(10):1263–1287

32. Sun Y, Jin J, Jing H, Lu Y, Zhu Q, Shu C, Zhang Q, Jing D (2021) ITIH4 is a novel serum biomarker for early gastric cancer diagnosis. Clin Chim Acta 523:365–373

33. Wang DD, Qian XK, Li HX, Jia GH, Jin Q, Luan X, Zhu YD, Wang YN, Huang J, Zou LW et al (2021) Sensing and imaging of exosomal CD26 secreted from cancer cells and 3D colorectal tumor model using a novel near-infrared fluorogenic probe. Mater Sci Eng C 130:112472

34. Yu C, Li L, Liu L, Wang Z, Zhu J (2021) Research of exosome in bone metastasis through dual aptamer recognition based entropy-driven amplification. Anal Biochem. 636:114433

35. Zhang Y, Wang Y, Su X, Wang P, Lin W (2021) The value of circulating circular RNA in cancer diagnosis, monitoring, prognosis, and guiding treatment. Front Oncol 11:736546

36. Zhao X, Guo X, Jiao D, Zhu J, Xiao H, Yang Y, Zhao S, Zhang J, Jiao F, Liu Z (2021) Analysis of the expression profile of serum exosomal lncRNA in breast cancer patients. Ann Transl Med 9(17):1382

37. Bobrie A, Colombo M, Krumeich S, Raposo G, Théry C (2012) Diverse subpopulations of vesicles secreted by different intracellular mechanisms are present in exosome preparations obtained by differential ultracentrifugation. J Extracell Vesicles. 1.

38. Konoshenko MY, Lekchnov EA, Vlassov AV, Laktionov PP (2018) Isolation of extracellular vesicles: general methodologies and latest trends. Biomed Res Int 2018:8545347

39. Tauro BJ, Greening DW, Mathias RA, Ji H, Mathivanan S, Scott AM, Simpson RJ (2012) Comparison of ultracentrifugation, density gradient separation, and immunoaffinity capture methods for isolating human colon cancer cell line LIM1863-derived exosomes. Methods (San Diego, Calif) 56(2):293–304

40. Livshits MA, Khomyakova E, Evtushenko EG, Lazarev VN, Kulemin NA, Semina SE, Generozov EV, Govorun VM (2015) Isolation of exosomes by differential centrifugation: theoretical analysis of a commonly used protocol. Sci Rep 5(1):17319

41. Maeki M, Kimura N, Sato Y, Harashima H, Tokeshi M (2018) Advances in microfluidics for lipid nanoparticles and extracellular vesicles and applications in drug delivery systems. Adv Drug Deliv Rev 128:84–100

42. Wang S, Zhang L, Wan S, Cansiz S, Cui C, Liu Y, Cai R, Hong C, Teng IT, Shi M et al (2017) Aptasensor with expanded nucleotide using DNA nanotetrahedra for electrochemical detection of cancerous exosomes. ACS Nano 11(4):3943–3949

43. Wang X, Shang H, Ma C, Chen L (2021) A fluorescence assay for exosome detection based on bivalent cholesterol anchor triggered target conversion and enzyme-free signal amplification. Anal Chem 93(24):8493–8500

44. Yuana Y, Levels J, Grootemaat A, Sturk A, Nieuwland R (2014) Co-isolation of extracellular vesicles and high-density lipoproteins using density gradient ultracentrifugation. J Extracell Vesicles. 3.

45. Wang A, Chan Miller C, Szostak JW (2019) Core-shell modeling of light scattering by vesicles: effect of size, contents, and lamellarity. Biophys J 116(4):659–669

46. Zougman A, Wilson JP, Banks RE (2020) A simple serum depletion method for proteomics analysis. Biotechniques 69(2):148–151

47. Oliveros, J.C. (2007-2015) Venny. An interactive tool for comparing lists with Venn's diagrams. [https://bioinfogp.cnb.csic.es/tools/venny/index.html]

48. Babicki S, Arndt D, Marcu A, Liang Y, Grant JR, Maciejewski A, Wishart DS (2016) Heatmapper: web-enabled heat mapping for all. Nucleic Acids Res 44(W1):W147-153

49. Metsalu T, Vilo J (2015) ClustVis: a web tool for visualizing clustering of multivariate data using principal component analysis and heatmap. Nucleic Acids Res 43(W1):W566–W570

50. Szklarczyk D, Gable AL, Nastou KC, Lyon D, Kirsch R, Pyysalo S, Doncheva NT, Legeay M, Fang T, Bork P et al (2021) The STRING database in 2021: customizable protein-protein networks, and functional characterization of user-uploaded gene/measurement sets. Nucleic Acids Res 49(D1):D605-d612

51. Liao Y, Wang J, Jaehnig EJ, Shi Z, Zhang B (2019) WebGestalt 2019: gene set analysis toolkit with revamped UIs and APIs. Nucleic Acids Res 47(W1):W199–W205

52. Feingold KR (2000): Introduction to lipids and lipoproteins. In: Feingold KR, Anawalt B, Boyce A, Chrousos G, de Herder WW, Dhatariya K, Dungan K, Hershman JM, Hofland J, Kalra S et al (Eds). South Dartmouth (MA): MDText.com, Inc. Copyright © 2000–2021, MDText.com, Inc.; *Endotext.* edn.

53. Woods D, Turchi JJ (2013) Chemotherapy induced DNA damage response: convergence of drugs and pathways. Cancer Biol Ther 14(5):379–389

54. Conklin KA (2004) Chemotherapy-associated oxidative stress: impact on chemotherapeutic effectiveness. Integr Cancer Ther 3(4):294–300

55. Chen Y, McMillan-Ward E, Kong J, Israels SJ, Gibson SB (2008) Oxidative stress induces autophagic cell death independent of apoptosis in transformed and cancer cells. Cell Death Differ 15(1):171–182

56. Ciocca DR, Calderwood SK (2005) Heat shock proteins in cancer: diagnostic, prognostic, predictive, and treatment implications. Cell Stress Chaperones 10(2):86–103

57. Gibert B, Hadchity E, Czekalla A, Aloy MT, Colas P, Rodriguez-Lafrasse C, Arrigo AP, Diaz-Latoud C (2011) Inhibition of heat shock protein 27 (HspB1) tumorigenic functions by peptide aptamers. Oncogene 30(34):3672–3681

58. Gibert B, Eckel B, Gonin V, Goldschneider D, Fombonne J, Deux B, Mehlen P, Arrigo AP, Clézardin P, Diaz-Latoud C (2012) Targeting heat shock protein 27 (HspB1) interferes with bone metastasis and tumour formation in vivo. Br J Cancer 107(1):63–70

59. Hansen RK, Parra I, Lemieux P, Oesterreich S, Hilsenbeck SG, Fuqua SAW (1999) Hsp27 overexpression inhibits doxorubicin–induced apoptosis in human breast cancer cells. Breast Cancer Res Treat 56(2):185–194

60. Vargas-Roig LM, Gago FE, Tello O, Aznar JC, Ciocca DR (1998) Heat shock protein expression and drug resistance in breast cancer patients treated with induction chemotherapy. Int J Cancer 79(5):468–475

61. Simonsen JB (2017) What are we looking at? Extracellular vesicles, lipoproteins, or both? Circ Res 121(8):920–922

62. Moman RN, Varacallo M (2019) Physiology, Albumin. StatPearls Publishing, Treasure Island

63. Ahmed N, Barker G, Oliva K, Garfin D, Talmadge K, Georgiou H, Quinn M, Rice G (2003) An approach to remove albumin for the proteomic analysis of low abundance biomarkers in human serum. Proteomics 3(10):1980–1987

64. Fu Q, Garnham CP, Elliott ST, Bovenkamp DE, Van Eyk JE (2005) A robust, streamlined, and reproducible method for proteomic analysis of serum by delipidation, albumin and IgG depletion, and two-dimensional gel electrophoresis. Proteomics 5(10):2656–2664

65. Steel LF, Trotter MG, Nakajima PB, Mattu TS, Gonye G, Block T (2003) Efficient and specific removal of albumin from human serum samples. Mol Cell Proteom 2(4):262–270

66. Melo SA, Luecke LB, Kahlert C, Fernandez AF, Gammon ST, Kaye J, LeBleu VS, Mittendorf EA, Weitz J, Rahbari N et al (2015) Glypican-1 identifies cancer exosomes and detects early pancreatic cancer. Nature 523(7559):177–182

67. Konig L, Kasimir-Bauer S, Bittner AK, Hoffmann O, Wagner B, Santos Manvailer LF, Kimmig R, Horn PA, Rebmann V (2017) Elevated levels of extracellular vesicles are associated with therapy failure and disease progression in breast cancer patients undergoing neoadjuvant chemotherapy. Oncoimmunology 7(1):e1376153

68. Midekessa G, Godakumara K, Ord J, Viil J, Lättekivi F, Dissanayake K, Kopanchuk S, Rinken A, Andronowska A, Bhattacharjee S et al (2020) Zeta potential of extracellular vesicles: toward understanding the attributes that determine colloidal stability. ACS Omega 5(27):16701–16710

69. Bæk R, Søndergaard EK, Varming K, Jørgensen MM (2016) The impact of various preanalytical treatments on the phenotype of small extracellular vesicles in blood analyzed by protein microarray. J Immunol Methods 438:11–20

70. Denkert C, Loibl S, Noske A, Roller M, Müller BM, Komor M, Budczies J, Darb-Esfahani S, Kronenwett R, Hanusch C et al (2010) Tumor-associated lymphocytes as an independent predictor of response to neoadjuvant chemotherapy in breast cancer. J Clin Oncol 28(1):105–113

Publisher's Note Springer Nature remains neutral with regard to jurisdictional claims in published maps and institutional affiliations.

Authors and Affiliations

Folnetti A. Alvarez[1] · **Hussein Kaddour**[1,2] · **Yuan Lyu**[1,3] · **Christina Preece**[4,5] · **Jules Cohen**[6,7] · **Lea Baer**[6,7] · **Alison T. Stopeck**[6,7] · **Patricia Thompson**[4,7] · **Chioma M. Okeoma**[1,8]

Folnetti A. Alvarez
folnetti.alvarez@stonybrook.edu

Hussein Kaddour
hussein.kaddour@regeneron.com

Yuan Lyu
lvyuan10@outlook.com

Christina Preece
Christina.Preece@stonybrookmedicine.edu

Jules Cohen
Jules.cohen@stonybrookmedicine.edu

Lea Baer
Lea.baer@stonybrookmedicine.edu

Alison T. Stopeck
Alison.stopeck@stonybrookmedicine.edu

Patricia Thompson
Patricia.Thompson@cshs.org;
Patricia.Carino@stonybrookmedicine.edu

[1] Department of Pharmacology, Stony Brook University Renaissance School of Medicine, Stony Brook, NY 11794-8651, USA

[2] Present Address: Regeneron Pharmaceuticals, Inc, Tarrytown, NY 10591, USA

[3] Present Address: Medical Research Center, The Third Affiliated Hospital of Zhengzhou University, Zhengzhou 450052, China

[4] Department of Pathology, Stony Brook University Renaissance School of Medicine, Stony Brook, NY 11794-8651, USA

[5] Present Address: Department of Medicine, Cedars Sinai Medical Center, Los Angeles, CA 90048, USA

[6] Department of Medicine, Division of Hematology and Medical Oncology, Stony Brook University, Stony Brook, NY 11794-8651, USA

[7] Stony Brook University Cancer Center, Stony Brook, NY 11794-8651, USA

[8] Present Address: Department of Pathology, Microbiology, and Immunology, New York Medical College, Valhalla, NY 10595-1524, USA